

Extended Results

Molecular modeling of mVP24 based on an eVP24 crystal structure. Filoviral VP24 proteins show significant sequence homology (data not shown). In order to gain insight into the structural basis for filoviral VP24 functions, we solved the crystal structure of the highly pathogenic Zaire EBOV VP24 protein (eVP24) (**Fig. S2, and Table S1** for structure statistics). Overall, the eVP24 structure adopts a conformation that is similar to those previously observed for the Reston virus and Sudan virus VP24 proteins (rVP24 and sVP24) (Zhang et al., 2012). In addition to the increased resolution to 1.92Å (compared to 2.0 Å and 2.1 Å rVP24 and sVP24 structures, respectively), many loop regions are experimentally well-defined in the eVP24 structure, particularly the residues that correspond to the mVP24 K-loop. For this reason, we chose to use the eVP24 structure for 1:1 threading using the mVP24 sequence. The resulting structure, shown in Fig. 1E, reveals that the critical K-loop of mVP24 is solvent exposed and is likely available to interact with the Keap1 Kelch domain. Previous studies of Keap1 Kelch interacting partners, such as Neh2 DLG, Neh2 ETGE, and p62, show that the peptide region binding to Kelch must be in an unfolded conformation (Cino et al., 2013). Consistent with these previous observations, our threaded model of mVP24 K-loop is predicted to be in a flexible conformation. While this data agrees with our binding studies and in vivo observations, additional structural data are required to experimentally confirm this observation.

mVP24 relocalizes Nrf2 to the nucleus. To determine whether interaction of mVP24 with the Keap1 Kelch domain activates Nrf2, a GFP-Nrf2 fusion protein was expressed alone or in the presence of Flag-Keap1 and HA-tagged wild-type mVP24, mutant mVP24 or wild-type or chimeric eVP24s. Over-expression of Nrf2, which overcomes endogenous Keap1, resulted in nuclear localization of GFP-Nrf2 (Fig. S1). Co-expression of Keap1 retained most of the Nrf2 in the cytoplasm. Additional expression of mVP24 restored Nrf2 nuclear localization in 72% of cells, suggesting disruption of the Nrf2-Keap1 interaction (**Fig. S1**). mVP24 linker, mVP24

D205A/E207A or mVP24 G211A/E212A did not prevent Keap1 retention of Nrf2 in the cytoplasm (Fig. S1). Expression of eVP24 also did not alter the cytoplasmic localization of Nrf2, but eVP24 K-loop resulted in 38% of cells having nuclear Nrf2 (**Fig. S1**). eVP24 DIEPCCGE, which precipitated less efficiently with Keap1 (**Fig. 1G**), was unable to relocalize Nrf2 to the nucleus (**Fig. S1**). Cumulatively, these data correlate mVP24-Keap1 interaction with the nuclear accumulation of Nrf2 and demonstrate that the presence of mVP24 can dissociate Nrf2 from Keap1.

Impact of HO-1 expression on a MARV minigenome assay. A recent study indicated that HO-1 expression inhibits EBOV replication/transcription (Hill-Batorski et al., 2013). As HO-1 is highly induced by MARV (**Fig. 4A**), we asked whether HO-1 expression affects MARV replication/transcription. When HO-1 was expressed in increasing amounts in the context of a MARV minigenome assay, no inhibitory effect was seen relative to a GFP over-expression control (**Fig. S4**). These results suggest that HO-1 expression may not affect MARV replication/transcription in the manner recently described for EBOV.

Extended Discussion

We demonstrate that mVP24 interacts comparably with bat Keap1 and human Keap1 (**Fig. 1**). The conservation of the mVP24 interaction with bat Keap1 is consistent with a role for this interaction in MARV reservoir hosts. Although the Egyptian fruit bat (*Rousettus aegyptiacus*) is the most definitive host species for MARV, its Keap1 sequence was not available. We were able to obtain from public databases the predicted sequences of an Old World fruit bat (*Pteropus alecto*) and a New World insectivorous bat (*Myotis lucifugus*). Each of these was highly conserved across its entire length with human Keap1. Therefore, we presume that the Egyptian fruit bat Keap1 will also be highly conserved relative to human Keap1. Based on the *M. lucifugus* Keap1 sequence, we cloned Keap1 from an available *Myotis velifer incautus* cell line and demonstrated that the interaction with mVP24 is conserved. Further, because bat

Keap1 is very similar to human Keap1, we were able to test the functional implications of mVP24 for bat Keap1 in human cells, confirming that mVP24 can disrupt bat Keap1-(human) Nrf2 interaction. Pathogenesis of MARV in humans is almost certainly different than in the reservoir host. It is worth considering, therefore, that the mVP24-Keap1 interaction may have unique consequences in bats versus humans.

Oxidative stress responses upon MARV infection have not been characterized. We demonstrate that the expression of mVP24 as well as MARV infection can upregulate a number of Nrf2 targeted genes, whereas EBOV infection did not result in a comparable induction over time. Although the response of ARE genes to MARV versus EBOV infection is clearly different, not all of our chosen ARE genes were upregulated by MARV infection. Our list of ARE genes was based on 30 genes that were induced in lymphoid cells treated with the dietary isothiocyanate, sulforaphane (SFN) (Chorley et al., 2012). As some studies report that different activators of Nrf2 can upregulate different subsets of genes in the same cell type (Lau et al., 2013), it may not be surprising that all 30 genes did not increase. As would be expected for a functionally significant interaction, two different strains of MARV were able to upregulate an ARE response, as demonstrated by induction of two of the best characterized ARE genes, HO-1 and GCLM. Numerous effects of HO-1 expression have been described, including protection from apoptosis, modulation of the NF κ B pathway and activation of the p38 mitogen-activated protein kinase (MAPK) pathway (reviewed in (Gozzelino et al., 2010)). GCLM is involved in the synthesis of glutathione, one of the major antioxidants in the cell (Ma, 2013). We hypothesize that upregulation of these, and other Nrf2 targeted genes, will enhance survival of MARV-infected cells, facilitating viral production.

Our data demonstrate that MARV and EBOV differ with regard to how they interact with the Nrf2 pathway. This is consistent with other functionally significant differences between these filoviral genera. Previously important differences have been described between MARV and

EBOV, including different mechanisms by which they inhibit innate immune responses. For example, eVP24 has been shown to interact with members of the NPI-1 subfamily of karyopherin alpha proteins to inhibit interferon signaling, but MARV VP24 does not (Mateo et al., 2009; Reid et al., 2006; Reid et al., 2007; Valmas et al., 2010). While MARV VP40 inhibits IFN signaling by blocking Jak1 function, EBOV VP40 does not (Valmas et al., 2010). Further, differences in the binding of MARV and EBOV VP35s to dsRNA suggest differences in how each virus antagonizes RIGI-like receptor signaling (Kimberlin et al., 2010; Leung et al., 2009; Leung et al., 2010a; Leung et al., 2010b; Ramanan et al., 2012b). Our data provides further evidence that there are significant differences between MARV and EBOV, despite the two viruses being in the same family.

Interestingly, HO-1 was recently reported to inhibit EBOV replication and inhibit an EBOV minigenome assay (Hill-Batorski et al., 2013). When we tested HO-1 expression for inhibitory activity towards a MARV minigenome assay, no suppressive activity was detected (Fig. S4). Inhibition of ARE responses by EBOV may suppress an anti-EBOV activity of HO-1. If MARV is resistant to the effects of HO-1, this may allow induction of HO-1 and other Nrf2-responsive genes for the purpose of enhancing cell survival.

The full implications of mVP24 interaction with Keap1 and a complete testing of the hypothesis that the interaction serves primarily to activate a cytoprotective state will require further study (see Discussion in main text). Nonetheless, some conclusions can be made. The induction of a cytoprotective state through the upregulation of ARE gene transcription would require the efficient translation of these cellular mRNAs. Because filoviruses do not shut down host cell transcription or protein synthesis, the ARE transcriptional response in MARV infected cells should lead to expression of cytoprotective proteins (Elliott et al., 1985; Hartman et al., 2008). Our hypothesis requires that infected cells survive long enough that virus yield can be enhanced. While little is known about MARV replication in the reservoir bat host, in many

human cell lines, the filovirus replication cycle is not particularly fast, and cells infected with EBOV have even been shown to undergo mitosis, demonstrating that these infections do not completely disrupt cellular processes (Hoenen et al., 2012). Therefore, the cytoprotective response would seem to have sufficient opportunity to be established during MARV infection. Also to be determined is whether other MARV proteins may modulate mVP24-Keap1 interaction.

It is notable that eVP24 seems to exert an inhibitory effect towards Nrf2-induced gene expression (**Fig. S3D**). The basis for this inhibition is unclear. This inhibitory activity may explain why the eVP24 chimeras containing mVP24 K-loop sequences do not activate ARE gene expression as well as wildtype mVP24 (**Fig. S3B and C**). Presumably, these eVP24 chimeras, which bind Keap1 efficiently, have two competing functions, an Nrf2 activating function (due to the interaction with Keap1) and an as yet unexplained inhibitory activity.

Filoviral VP24s also interact with filoviral VP35 and NP proteins in viral nucleocapsids, modulate viral RNA synthesis and play roles in viral budding (Bamberg et al., 2005; Beniac et al.; Bharat et al., 2012; Bharat et al., 2011; Hoenen et al., 2006; Huang et al., 2002; Mateo et al.; Noda et al., 2006; Watanabe et al., 2007; Wenigenrath et al., 2010). Further study will be required to understand the interplay and functional consequences of the various mVP24 interactions. A more complete understanding of these issues may suggest novel antiviral approaches to these deadly viruses.

Extended Experimental Procedures

Cells

HEK293T, HeLa and *Myotis velifer incautus* (ATCC, CRL-6012) cell lines were maintained in Dulbecco's minimal essential medium supplemented with 10% fetal bovine serum (FBS) and

cultured at 37°C and 5% CO₂. BSRT7 cells were grown in the same medium supplemented with 1% G418. THP-1 cells were maintained in RPMI supplemented with 10% FBS, 1% penicillin/streptomycin, 1% L-glutamine, 1% sodium pyruvate and 1% beta mercaptoethanol.

Plasmids

The plasmids encoding Flag and HA tagged mVP24 and eVP24 in the pCAGGS vector were previously described (Valmas et al., 2010). Mutations to mVP24 were made using overlapping PCR and cloned into pCAGGS vector containing a N-terminal Flag tag. Mutations of residues to alanines were done using the GCT codon. The serine/glycine linker, SGGSGGSG, in the mVP24 linker mutant was inserted into mVP24 using the forward primer 5'-TCCGGAGGCTCAGGTGGCAGCGGAacagtcctctcagaatcag-3' and the reverse primer 5'-TCCGCTGCCACCTGAGCCTCCGGAaatcctctgactccac-3' (the serine/glycine linker sequence is in capital letters). mVP24 residues 205-DIEPCCGE-212 were inserted into eVP24 between residues 202 and 211 using overlapping PCR, making eVP24 DIEPCCGE. mVP24 residues 202-RRIDIEPCCGETVLSESV-219 were inserted into eVP24 between residues 201 and 218 using overlapping PCR, making eVP24 K-loop. pcDNA Flag tagged Keap1 was purchased from Addgene (Addgene plasmid 28023(Fan et al., 2010)) and cloned with an N-terminal Flag tag into pCAGGS. A series of domain deletion mutants of Keap1 in Flag tagged pCAGGS were constructed by PCR. Keap1 Δ NTR construct lacks the first 60 amino acids, Keap1 Δ IVR lacks amino acids 180-314 and Keap1 Δ Kelch/CTR lacks amino acids 315-624. Keap1 Kelch/CTR contains amino acids 315-624. Flag tagged Keap1 R415A was generated using overlapping PCR and the GCC codon to make the mutation to alanine. pcDNA3Myc tagged Nrf2 was purchased from Addgene (Addgene plasmid 21555(Furukawa and Xiong, 2005)) and cloned with an N-terminal HA tag or Flag tag into pCAGGS or into a pCAGGS GFP fusion construct. pcDNA4/TO HA p62 was purchased from Addgene (Addgene plasmid 28027). The pGL4.37[*luc2P*/ARE/Hygro] (ARE) reporter was purchased from Promega. HO-1 was cloned

using cDNA from THP-1 isolated RNA and the forward primer 5'-atggagcgtccgcaacccgac-3' and reverse primer 5'-tcacatggcataaagccctac-3' and inserted into pCAGGS such that it is expressed with an N-terminal HA tag. Bat-Keap1 and bat-Kelch were amplified from *Myotis velifer incautus* cell mRNA. For full length Keap1, forward primer 5'-atgcagccggaacccgggccc-3' and for the Kelch domain forward primer 5'-caggtgatgccctgccgg-3' were used. Each construct was amplified by using the same reverse primer 5'-tcaacaggtacagttctgctgg-3'. These amplicons were cloned into pCAGGS vector such that they produced a protein with an N-terminal Flag tag. MARV L was synthesized and cloned into pCAGGS such that it expressed with an N-terminal Flag tag. Flag-VP35 and Flag-NP have been previously described (Ramanan et al., 2012a).

Antibodies

Monoclonal mouse anti-FLAG M2 antibody, polyclonal rabbit anti-Flag antibody, monoclonal mouse anti-HA antibody and a polyclonal rabbit anti-HA antibody were purchased from Sigma-Aldrich. A mouse monoclonal anti-NQO1 (A180) antibody was purchased from Santa Cruz. Alexa Fluor anti-mouse 555 and Alexa Fluor anti-rabbit 633 were purchased from Invitrogen.

Isothermal Titration Calorimetry. All proteins were extensively dialyzed against buffer containing 10 mM HEPES (pH 7.0.), 150 mM sodium chloride, and 2 mM tris(2-carboxyethyl)phosphine and degassed before use. 110 μ M Keap1 Kelch domain protein was loaded into a stirring syringe and injected into a sample cell containing 5 μ M Nrf2 Neh2 domain protein or 7 μ M mVP24 protein. Binding data were analyzed using Origin (OriginLab). The binding stoichiometry (n), enthalpy change (ΔH), entropy change (ΔS), and binding association constant (K_a) were obtained from the experimental titration curve. Dissociation constants (K_D) were calculated from the K_a .

Immunofluorescence

HeLa cells grown on glass coverslips were transfected with indicated plasmids using Lipofectamine 2000 (Invitrogen). At 24 hours post transfection, cells were fixed using 4% paraformaldehyde and permeabilized using 0.1% Triton X-100. Cells were stained using the primary antibodies to Flag M2 (dilution 1:400) and HA (dilution 1:400) and secondary antibodies conjugated to Alexa Fluor 555 or Alexa Fluor 633 (Life Technologies) (dilution 1:2000). Images were taken using Zeiss Axioplan 2IE fluorescence microscope. The percent of cells containing nuclear Nrf2 localization was determined by counting cells in four individual fields of view.

Cell viability assay

HEK293T cells (10,000) were transfected using Lipofectamine 2000 (Invitrogen) with pCAGGS, Flag-Nrf2, mVP24 or mVP24 G211A/E212A plasmids. At 24 hours post transfection cells were treated with a vehicle control (ethanol) or 5uM of menadione (Sigma) for three hours, after which cells were assayed using CellTiter-Glo luminescent cell viability assay (Promega). The assay was performed with six replicates; error bars represent the SEM. Statistical analysis was done by one-way ANOVA using Tukey's test, * $p < 0.05$.

Western Blotting

Lysates were run on 10% acrylamide SDS/PAGE gels (Lonza) and transferred to polyvinylidenedifluoride membrane. The membranes were probed with anti-FLAG M2, anti-HA and/or anti-NQO1 and developed using Western Lightning ECL kit (Perkin-Elmer).

RNA extractions and qRT-PCR

HEK293T cells (2.5×10^5) were transfected using Lipofectamine 2000 (Invitrogen) with the indicated plasmids. Cells were harvested at 24 hours post transfection. RNA was extracted using the RNeasy Kit (Qiagen), and cDNA was generated using SuperScript III Reverse Transcriptase (Invitrogen). Primers used for qRT-PCR were previously described (Lau et al.,

2010). Transfections were performed in triplicate and the data were expressed as relative mRNA levels normalized to RPS11.

MARV minigenome assay

BSRT7 cells (2.5×10^5) were transfected in triplicate using Lipofectamine 2000 (Invitrogen) with the MARV minigenome plasmid (encoding *Renilla* luciferase) (200ng), a plasmid with firefly luciferase under the control of the T7 promoter as a transfection control (10ng), and plasmids encoding MARV L (500ng), MARV VP35 (125 ng) and MARV NP (500 ng). HA-HO-1 or GFP was co-transfected at increasing concentrations (100 ng, 500 ng and 1 μ g). Forty-eight hours post-transfection a Dual luciferase assay (Promega) was performed. *Renilla* luciferase values were normalized to firefly luciferase values. Error bars represent the mean and SEM of triplicate samples, and statistical significance was assessed by a one-way ANOVA comparing bars as indicated using Tukey's test.

eVP24 cloning, expression, and purification

eVP24 was subcloned into a modified pET15b vector (Novagen) and sequenced before use. eVP24 was overexpressed as an MBP fusion protein in BL21(DE3) *E. coli* cells (Novagen) in LB medium. Protein expression was induced at an OD_{600nm} of 0.6 with 0.5 mM IPTG (Sigma) at 18°C. Cells were harvested, resuspended in buffer containing 25 mM sodium phosphate pH 7.5, 250 mM NaCl, 20 mM imidazole, and 5 mM 2-mercaptoethanol, and lysed using an EmulsiFlex-C5 homogenizer (Avestin). Cell lysate was clarified by centrifugation at 30,000 x *g* at 4 °C for 30 min. eVP24 protein was purified using a series of chromatographic columns. The MBP fusion tag was cleaved with TEV protease prior to loading on a Superdex 75 gel filtration column (GE Healthcare). Sample purity was determined by SDS-PAGE.

eVP24 crystallization, x-ray data collection, and structure determination

Initial crystallization conditions were obtained using commercially available screens (Hampton

Research) and by the hanging drop method. Initial hits were further optimized using in-house reagents. Diffraction quality crystals were obtained in 150 mM MES pH 5.4, 20% Jeffamine M-600 pH 7.0, 50 mM CaCl₂, and 6 mM LiCl using 15 mg/ml of eVP24 protein. Crystals were cryo-protected with 25% glycerol prior to vitrification. X-ray diffraction data were collected at the Advanced Light Source (ALS) beamline 4.2.2 (Berkeley, CA) initially and the final data were collected at the Advanced Photon Source (APS) beamline 19ID (Argonne, IL). The best eVP24 crystal diffracted to 1.92 Å. Diffraction data was processed using HKL3000 (Otwinowski and Minor, 1997). The structure was solved by molecular replacement with Molrep using PDB ID 3VNE and 4D9O as the search model and refined using REFMAC5 (Vagin et al, 2004). Manual model building was done in COOT (Emsley et al, 2004) with additional refinement using PHENIX1.8.2 (Adams, P.D, et al, 2010). The structure quality was assessed using MolProbity (Davis I. W et al, 2007).

In vitro pull-down assays.

Pull-down assays were performed in buffer containing 20 mM Tris-HCl (pH 7.0), 50 mM sodium chloride, and 2 mM tris(2-carboxyethyl)phosphine. MBP-fusion mVP24 protein was immobilized on amylose resin prior to the addition of Keap1 Kelch domain and Nrf2 Neh2 domain. Bound resin was washed extensively. Samples were visualized by Coomassie blue staining of SDS-PAGE gels.

Supplemental References

Bamberg, S., Kolesnikova, L., Moller, P., Klenk, H.D., and Becker, S. (2005). VP24 of Marburg virus influences formation of infectious particles. *J Virol* 79, 13421-13433.

Beniac, D.R., Melito, P.L., Devarenes, S.L., Hiebert, S.L., Rabb, M.J., Lamboo, L.L., Jones, S.M., and Booth, T.F. (2012). The organisation of Ebola virus reveals a capacity for extensive, modular polyploidy. *PLoS One* 7, e29608.

Bharat, T.A., Noda, T., Riches, J.D., Kraehling, V., Kolesnikova, L., Becker, S., Kawaoka, Y., and Briggs, J.A. (2012). Structural dissection of Ebola virus and its assembly determinants using cryo-electron tomography. *Proc Natl Acad Sci U S A* 109, 4275-4280.

Bharat, T.A., Riches, J.D., Kolesnikova, L., Welsch, S., Kraehling, V., Davey, N., Parsy, M.L., Becker, S., and Briggs, J.A. (2011). Cryo-electron tomography of Marburg virus particles and their morphogenesis within infected cells. *PLoS Biol* 9, e1001196.

Chorley, B.N., Campbell, M.R., Wang, X., Karaca, M., Sambandan, D., Bangura, F., Xue, P., Pi, J., Kleeberger, S.R., and Bell, D.A. (2012). Identification of novel NRF2-regulated genes by ChIP-Seq: influence on retinoid X receptor alpha. *Nucleic Acids Res* 40, 7416-7429.

Cino, E.A., Killoran, R.C., Karttunen, M., and Choy, W.Y. (2013). Binding of disordered proteins to a protein hub. *Sci Rep* 3, 2305.

Elliott, L.H., Kiley, M.P., and McCormick, J.B. (1985). Descriptive analysis of Ebola virus proteins. *Virology* 147, 169-176.

Fan, W., Tang, Z., Chen, D., Moughon, D., Ding, X., Chen, S., Zhu, M., and Zhong, Q. (2010). Keap1 facilitates p62-mediated ubiquitin aggregate clearance via autophagy. *Autophagy* 6, 614-621.

Furukawa, M., and Xiong, Y. (2005). BTB protein Keap1 targets antioxidant transcription factor Nrf2 for ubiquitination by the Cullin 3-Roc1 ligase. *Molecular and cellular biology* 25, 162-171.

Gozzelino, R., Jeney, V., and Soares, M.P. (2010). Mechanisms of cell protection by heme oxygenase-1. *Annu Rev Pharmacol Toxicol* 50, 323-354.

Hartman, A.L., Ling, L., Nichol, S.T., and Hibberd, M.L. (2008). Whole-genome expression profiling reveals that inhibition of host innate immune response pathways by Ebola virus can be reversed by a single amino acid change in the VP35 protein. *J Virol* *82*, 5348-5358.

Hill-Batorski, L., Halfmann, P., Neumann, G., and Kawaoka, Y. The Cytoprotective Enzyme Heme Oxygenase-1 Suppresses Ebola virus Replication. *J Virol*.

Hill-Batorski, L., Halfmann, P., Neumann, G., and Kawaoka, Y. (2013). The Cytoprotective Enzyme Heme Oxygenase-1 Suppresses Ebola Virus Replication. *Journal of virology* *87*, 13795-13802.

Hoenen, T., Groseth, A., Kolesnikova, L., Theriault, S., Ebihara, H., Hartlieb, B., Bamberg, S., Feldmann, H., Stroher, U., and Becker, S. (2006). Infection of naive target cells with virus-like particles: implications for the function of ebola virus VP24. *J Virol* *80*, 7260-7264.

Hoenen, T., Shabman, R.S., Groseth, A., Herwig, A., Weber, M., Schudt, G., Dolnik, O., Basler, C.F., Becker, S., and Feldmann, H. Inclusion bodies are a site of ebolavirus replication. *J Virol* *86*, 11779-11788.

Hoenen, T., Shabman, R.S., Groseth, A., Herwig, A., Weber, M., Schudt, G., Dolnik, O., Basler, C.F., Becker, S., and Feldmann, H. (2012). Inclusion bodies are a site of ebolavirus replication. *Journal of virology* *86*, 11779-11788.

Huang, Y., Xu, L., Sun, Y., and Nabel, G.J. (2002). The assembly of Ebola virus nucleocapsid requires virion-associated proteins 35 and 24 and posttranslational modification of nucleoprotein. *Mol Cell* *10*, 307-316.

Kimberlin, C.R., Bornholdt, Z.A., Li, S., Woods, V.L., Jr., MacRae, I.J., and Saphire, E.O. Ebolavirus VP35 uses a bimodal strategy to bind dsRNA for innate immune suppression. *Proc Natl Acad Sci U S A* *107*, 314-319.

Lau, A., Wang, X.J., Zhao, F., Villeneuve, N.F., Wu, T., Jiang, T., Sun, Z., White, E., and Zhang, D.D. (2010). A noncanonical mechanism of Nrf2 activation by autophagy deficiency: direct interaction between Keap1 and p62. *Mol Cell Biol* *30*, 3275-3285.

Lau, A., Zheng, Y., Tao, S., Wang, H., Whitman, S.A., White, E., and Zhang, D.D. (2013). Arsenic inhibits autophagic flux activating the Nrf2-Keap1 pathway in a p62-dependent manner. *Mol Cell Biol*.

Leung, D.W., Ginder, N.D., Fulton, D.B., Nix, J., Basler, C.F., Honzatko, R.B., and Amarasinghe, G.K. (2009). Structure of the Ebola VP35 interferon inhibitory domain. *Proc Natl Acad Sci U S A* *106*, 411-416.

Leung, D.W., Prins, K.C., Borek, D.M., Farahbakhsh, M., Tufariello, J.M., Ramanan, P., Nix, J.C., Helgeson, L.A., Otwinowski, Z., Honzatko, R.B., *et al.* (2010a). Structural basis for dsRNA recognition and interferon antagonism by Ebola VP35. *Nat Struct Mol Biol* *17*, 165-172.

Leung, D.W., Shabman, R.S., Farahbakhsh, M., Prins, K.C., Borek, D.M., Wang, T., Muhlberger, E., Basler, C.F., and Amarasinghe, G.K. (2010b). Structural and functional characterization of Reston Ebola virus VP35 interferon inhibitory domain. *J Mol Biol* *399*, 347-357.

Ma, Q. (2013). Role of nrf2 in oxidative stress and toxicity. *Annu Rev Pharmacol Toxicol* *53*, 401-426.

Mateo, M., Carbonnelle, C., Martinez, M.J., Reynard, O., Page, A., Volchkova, V.A., and Volchkov, V.E. (2011). Knockdown of Ebola virus VP24 impairs viral nucleocapsid assembly and prevents virus replication. *J Infect Dis* *204 Suppl 3*, S892-896.

Mateo, M., Reid, S.P., Leung, L.W., Basler, C.F., and Volchkov, V.E. (2009). Ebolavirus VP24 binding to karyopherins is required for inhibition of interferon signaling. *J Virol* *84*, 1169-1175.

Noda, T., Ebihara, H., Muramoto, Y., Fujii, K., Takada, A., Sagara, H., Kim, J.H., Kida, H., Feldmann, H., and Kawaoka, Y. (2006). Assembly and budding of Ebolavirus. *PLoS Pathog* *2*, e99.

Otwinowski, Z., and Minor, W. (1997). Processing of X-ray diffraction data collected in oscillation mode. *Methods Enzymol* *276*, 307-326.

Ramanan, P., Edwards, M.R., Shabman, R.S., Leung, D.W., Endlich-Frazier, A.C., Borek, D.M., Otwinowski, Z., Liu, G., Huh, J., Basler, C.F., *et al.* (2012a). Structural basis for Marburg virus VP35-mediated immune evasion mechanisms. *Proceedings of the National Academy of Sciences of the United States of America* *109*, 20661-20666.

Ramanan, P., Edwards, M.R., Shabman, R.S., Leung, D.W., Endlich-Frazier, A.C., Borek, D.M., Otwinowski, Z., Liu, G., Huh, J., Basler, C.F., *et al.* (2012b). Structural basis for Marburg virus VP35-mediated immune evasion mechanisms. *Proc Natl Acad Sci U S A* *109*, 20661-20666.

Reid, S.P., Leung, L.W., Hartman, A.L., Martinez, O., Shaw, M.L., Carbonnelle, C., Volchkov, V.E., Nichol, S.T., and Basler, C.F. (2006). Ebola virus VP24 binds karyopherin alpha1 and blocks STAT1 nuclear accumulation. *J Virol* *80*, 5156-5167.

Reid, S.P., Valmas, C., Martinez, O., Sanchez, F.M., and Basler, C.F. (2007). Ebola virus VP24 proteins inhibit the interaction of NPI-1 subfamily karyopherin alpha proteins with activated STAT1. *J Virol* *81*, 13469-13477.

Valmas, C., Grosch, M.N., Schumann, M., Olejnik, J., Martinez, O., Best, S.M., Krahling, V., Basler, C.F., and Muhlberger, E. (2010). Marburg virus evades interferon responses by a mechanism distinct from ebola virus. *PLoS Pathog* *6*, e1000721.

Watanabe, S., Noda, T., Halfmann, P., Jasenosky, L., and Kawaoka, Y. (2007). Ebola virus (EBOV) VP24 inhibits transcription and replication of the EBOV genome. *J Infect Dis* *196 Suppl* *2*, S284-290.

Wenigenrath, J., Kolesnikova, L., Hoenen, T., Mittler, E., and Becker, S. (2010). Establishment and application of an infectious virus-like particle system for Marburg virus. *J Gen Virol* *91*, 1325-1334.

Zhang, A.P., Bornholdt, Z.A., Liu, T., Abelson, D.M., Lee, D.E., Li, S., Woods, V.L., Jr., and Saphire, E.O. (2012). The ebola virus interferon antagonist VP24 directly binds STAT1 and has a novel, pyramidal fold. *PLoS Pathog* *8*, e1002550.

SUPPLEMENTAL TABLE

Table S1. Data collection, structure solution, and refinement statistics, related to Figure 2.

Data collection	
Space Group	$P4_32_12$
Unit cell parameters	
a, b, c (Å)	71.775, 71.775, 191.165
α, β, γ (°)	90, 90, 90
Resolution range (Å)	50 - 1.92
	(1.95 - 1.92)
Unique reflections	39161 (1923)
Redundancy	9.6 (9.7)
Completeness (%)	100.0(100.0)
R_{merge} (%)	8.9 (96.3)
$I / I\sigma$	33.2 (2.3)
Structure solution and refinement	
Resolution (Å)	33.60 - 1.92
	(1.97 - 1.92)
No. of reflections	39068
Completeness (%)	99.98 (99.90)
non-hydrogen atoms	3536
R_{work} / R_{free} (%)	20.21/22.93
	(24.88/28.62)
R.m.s. deviations	
Bond lengths (Å)	0.012
Bond angles (°)	1.575
B -factors (Å ²)	
Protein	
Chain A	44.75
Chain B	43.71
Water	45.29
Ramachandran plot outliers (%)	0.5
Molprobit score	2.02
Molprobit clash score	7.94

Experimental and refinement parameters were calculated as described in methods using standard methods. Values in parentheses are for the highest resolution shell 1.95 - 1.92 Å for data collection and for 1.97-1.92 Å for refinement.

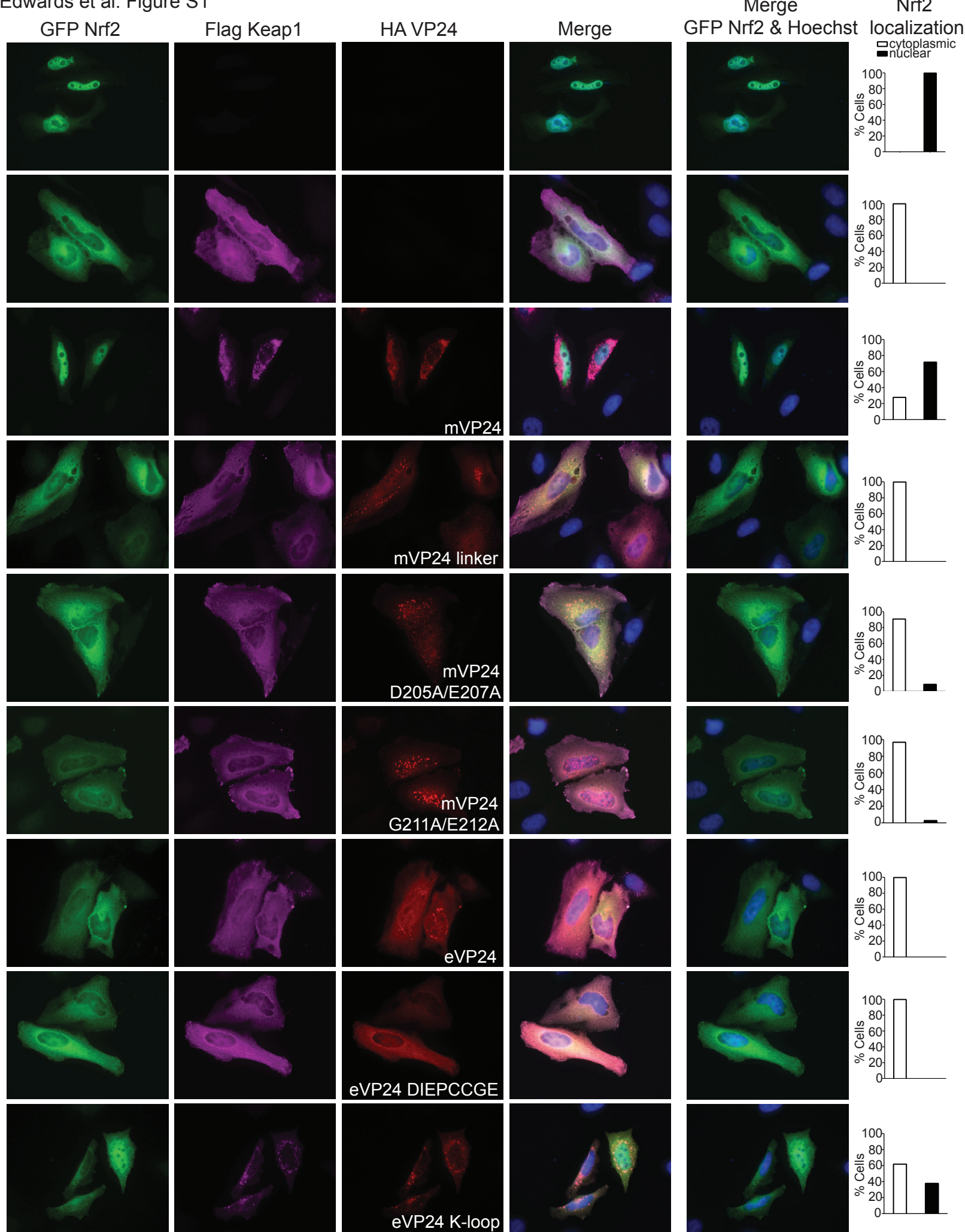
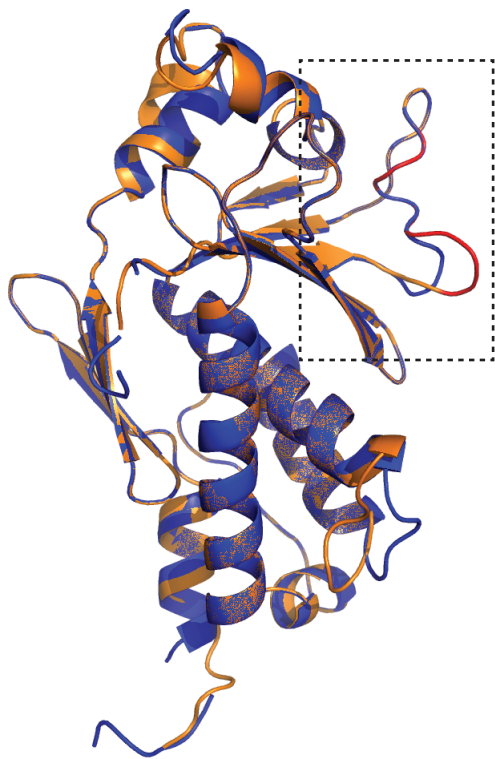
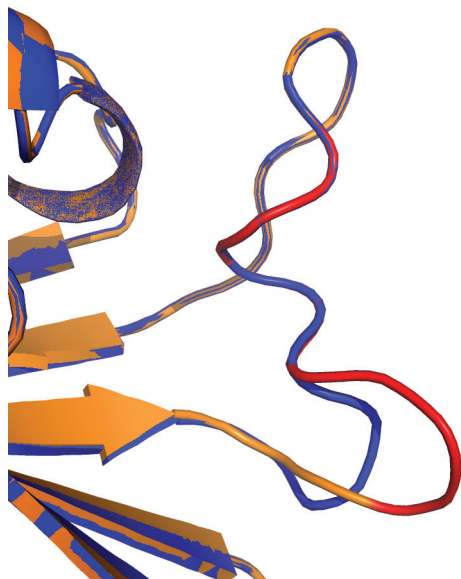


Fig. S1. mVP24 co-localizes with Keap1 and expression relocates Nrf2 to the nucleus, related to Figure 1. HeLa cells were transfected with plasmids for GFP-Nrf2, Flag-Keap1 and/or HA-tagged VP24 proteins. Twenty-four hours post transfection, slides were fixed and stained with anti-Flag antibody and anti-rabbit IgG Alexa Fluor 633 or anti-HA antibody and anti-mouse IgG Alexa Fluor 555 to visualize protein localization. Image is representative. The percent of cells with cytoplasmic vs. nuclear Nrf2 was determined by counting cells in four individual fields of view for each sample.

A



B

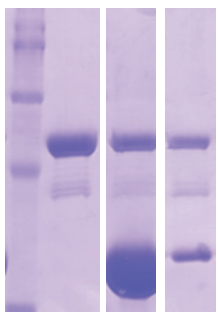


C

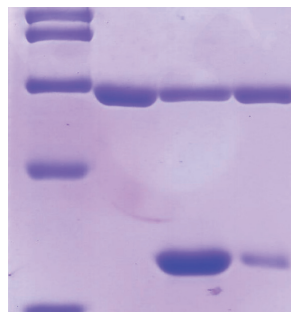
mVP24 ---²⁰²RRIDIEPCC²⁰⁵GETVL²¹²SES²¹⁹V---

eVP24 ---²⁰²QEPDKSAMDIRHPGPV²¹⁷---

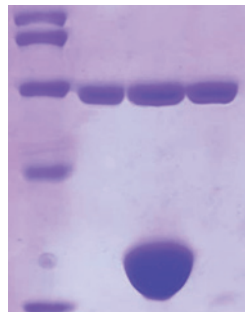
D



E



F



G

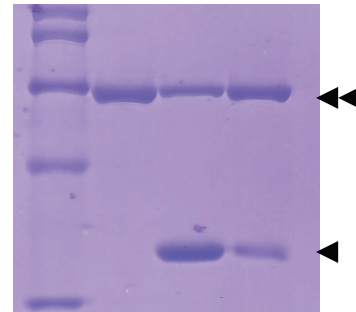
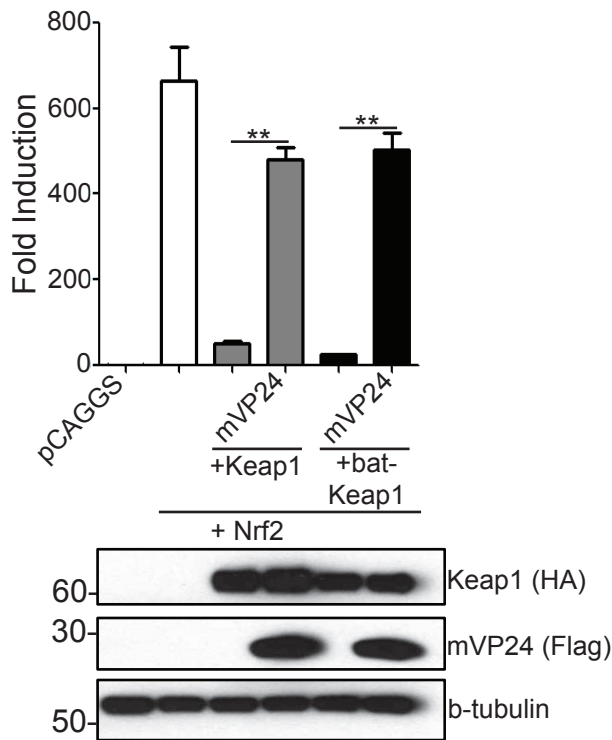
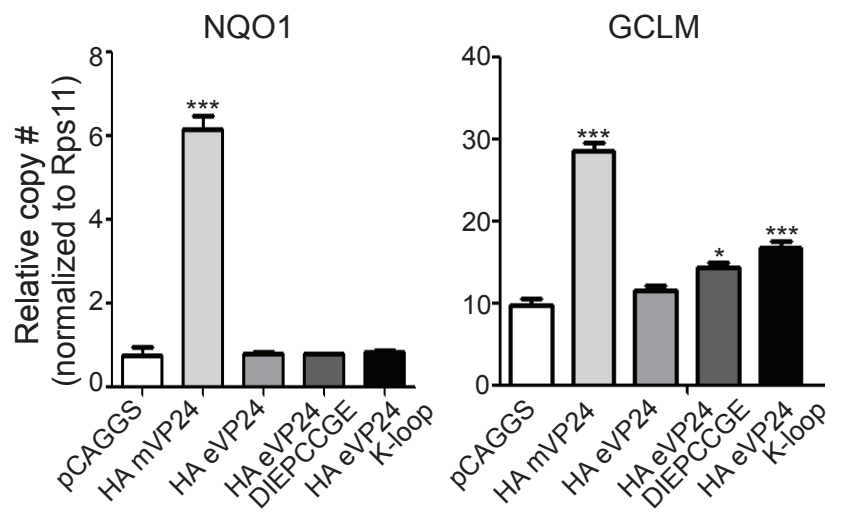


Fig. S2. mVP24 K-loop residues in the eVP24 scaffold are sufficient to mediate interactions between VP24 and the Keap1 Kelch domain, related to Figure 2. (A and B) Alignment of the Phyre2 generated structural model of mVP24 (orange) based on the eVP24 (purple) crystal structure (PDB ID 4M0Q). Residues in the K-loop are highlighted and expanded in (B). mVP24 K-loop residues 205-212 are highlighted in red. (C) Schematic representation of residues present in the loop regions of mVP24 and eVP24 highlighted in (B). (D, E, F and G) Coomassie blue-stained SDS-PAGE of pulldown assays of the Keap1 Kelch domain with: D. MBP-Nrf2 Neh2, E. MBP-mVP24, F. MBP-eVP24, and G. MBP-eVP24 K-loop. Lanes from left to right correspond to marker, amylose resin bound to MBP-tagged protein (double arrowheads), Keap1 Kelch domain (single arrowhead) added to amylose resin bound to MBP-tagged protein, and final bound amylose resin after washes.

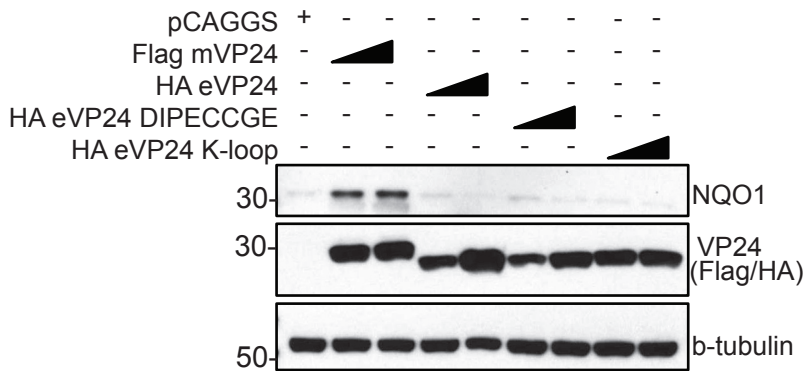
A



B



C



D

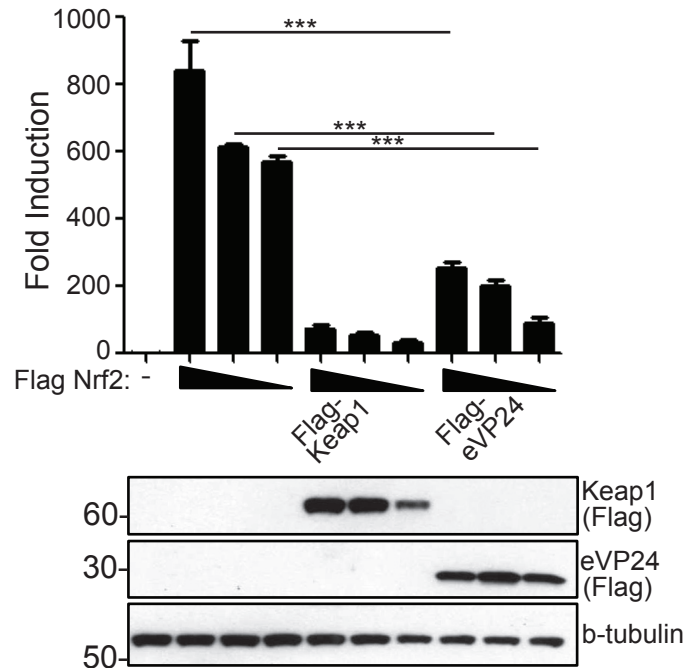


Fig. S3. Interaction of VP24 constructs with Keap1 activates ARE gene expression, related to Figure 3. 293T cells were transfected with the ARE luciferase reporter plasmid, a constitutively expressed *Renilla* luciferase plasmid, Flag-Nrf2, HA-Keap1 and pCAGGS (empty vector) or Keap1 or bat-Keap1 and Flag mVP24 as indicated. At 18 hpt luciferase activity was assayed. Western blots for HA and Flag are indicated. (B) pCAGGS, HA-mVP24, eVP24, eVP24 DIEPCCGE or eVP24 K-loop were transfected in triplicate in HEK293T cells. At 24 hpt, qRT-PCR was performed for the indicated mRNAs and normalized to *RPS11*. (C) 293T cells were transfected with the indicated plasmids, and 18 hpt endogenous NQO1 was measured by western blot. (D) The same assay protocol as in (A) but with Flag-Nrf2, Keap1 and eVP24 transfected as indicated. (A, B and D) represent the mean and SEM of triplicate samples, and statistical significance was assessed by a one-way ANOVA comparing columns to the control (white bar) or as indicated, *** $p < 0.001$, ** $p < 0.01$ and * $p < 0.05$.

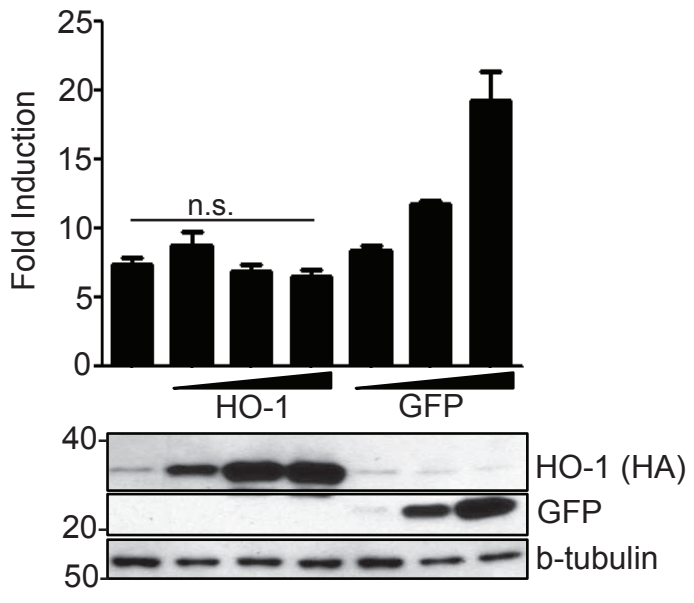


Fig. S4. MARV replication/transcription is not detectably affected by HO-1 expression, related to Figure 4. BSRT7 cells were transfected with the MARV *Renilla* luciferase minigenome, firefly luciferase as transfection control, and MARV L, VP35 and NP. HA-HO-1 or GFP were co-transfected at increasing concentrations (100ng, 500ng and 1ug). Forty-eight hpt luciferase activity was assayed. Bars represent the mean and SEM of triplicate samples and statistical significance was assessed by a one-way ANOVA comparing bars as indicated. n.s., no significance.